Combined Optical and Electrical Spectrum Shaping for High-Baud-Rate Nyquist-WDM Transceivers

Porto da Silva, Edson; Borkowski, Robert; Preussler, Stefan; Schwartau, Fabian; Gaiarin, Simone; Iglesias Olmedo, Miguel; Vedadi, Armand; Piels, Molly; Galili, Michael; Guan, Pengyu

Total number of authors:
15

Published in:
IEEE Photonics Journal

Link to article, DOI:
10.1109/JPHOT.2016.2523978

Publication date:
2016

Document Version
Publisher's PDF, also known as Version of record

IEEE Photonics Journal
An IEEE Photonics Society Publication

Open Access

Combined Optical and Electrical Spectrum Shaping for High-Baud-Rate Nyquist-WDM Transceivers

Volume 8, Number 1, February 2016

Edson P. da Silva
Robert Borkowski
Stefan Preußler
Fabian Schwartau
Simone Gaiarin
Miguel I. Olmedo
Armand Vedadi
Molly Piels
Michael Galili
Pengyu Guan
Sergei Popov
Camille-Sophie Brès
Thomas Schneider
Leif K. Oxenløwe
Darko Zibar

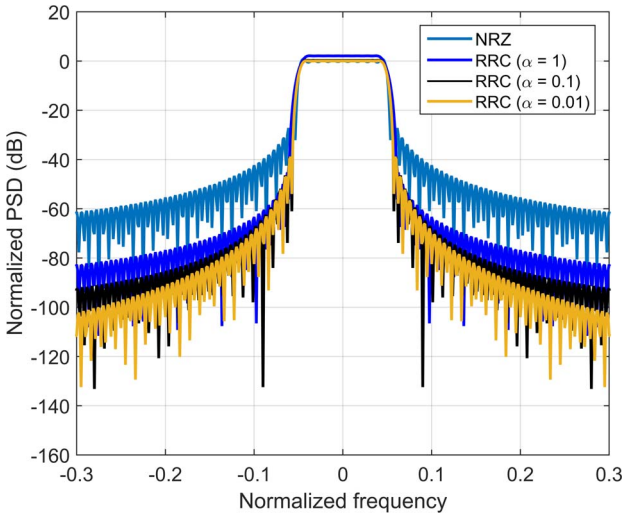

DOI: 10.1109/JPHOT.2016.2523978
1943-0655

Combined Optical and Electrical Spectrum Shaping for High-Baud-Rate Nyquist-WDM Transceivers

Edson P. da Silva,[1] Robert Borkowski,[1] Stefan Preußler,[2] Fabian Schwartau,[2] Simone Gaiarin,[1] Miguel I. Olmedo,[3] Armand Vedadi,[4] Molly Piels,[1] Michael Galili,[1] Pengyu Guan,[1] Sergei Popov,[3] Camille-Sophie Brès,[4] Thomas Schneider,[2] Leif K. Oxenløwe,[1] and Darko Zibar[1]

[1]DTU Fotonik, Technical University of Denmark (DTU), 2800 Lyngby, Denmark
[2]Technische Universität Braunschweig, 38106 Braunschweig, Germany
[3]KTH Royal Institute of Technology, 114 28 Stockholm, Sweden
[4]École Polytechnique Fédérale de Lausanne, 1015 Lausanne, Switzerland

DOI: 10.1109/JPHOT.2016.2523978

Manuscript received January 12, 2016; revised January 26, 2016; accepted January 28, 2016. Date of publication February 8, 2016; date of current version February 12, 2016. This work was supported in part by the Villum Foundation, Søborg, Denmark, and in part by the EU project ICONE under Grant 608099. Corresponding author: E. P. da Silva (e-mail: edpod@fotonik.dtu.dk).

Abstract: We discuss the benefits and limitations of optical time-division multiplexing (OTDM) techniques based on the optical generation of a periodic train of sinc pulses for wavelength-division multiplexing (WDM) transmission at high baud rates. It is shown how the modulated OTDM spectrum bandwidth is related to the optical comb parameters and the pulse shaping of the modulating waveforms in the electrical domain. Such dependence may result in broadening of the modulated spectra, which can degrade the performance of Nyquist-WDM systems due to interchannel crosstalk penalties. However, it is shown and experimentally demonstrated that the same technique of optical pulse train generation can be allied with digital pulse shaping to improve the confinement of the modulated spectrum toward the Nyquist limit independently of the number of OTDM tributaries used. To investigate the benefits of the proposed approach, we demonstrate the first WDM Nyquist-OTDM signal generation based on the periodic train of sinc pulses and electrical spectrum shaping. Straight line transmission of five 112.5-Gbd Nyquist-OTDM dual-polarization quadrature phase-shift keying (QPSK) channels is demonstrated over a dispersion uncompensated link up to 640 km, with full-field coherent detection at the receiver. It is shown that such a design strategy effectively improves the spectral confinement of the modulated OTDM signal, providing a minimum intercarrier crosstalk penalty of 1.5 dB in baud-rate-spaced Nyquist-WDM systems.

Index Terms: Coherent communications, Nyquist-OTDM.

1. Introduction

Historically, due to cost and complexity, industry has adopted single carrier based transceivers for optical wavelength division multiplexing (WDM) systems. Following this trend, and in order to comply with future capacity requirements for WDM networks, single-carrier transceivers based on high serial interface rates and advanced modulation formats are needed. Such architectures can be designed using different signal generation techniques. In [1], experimental

demonstrations of high baud rate transmission systems employing electrical time division multiplexing (ETDM), quadrature phase shift keying (QPSK), and quadrature amplitude modulation (QAM) are shown. Transmission of DP-QPSK and DP-16QAM at 107 GBd, and DP-64QAM at 72 GBd were demonstrated over dispersion uncompensated links. However, at such high ETDM rates (> 100 GBd), constraints on the bandwidth of digital-to-analog converters (DAC) and electrical multiplexers (MUX) impose challenges to increase the spectral efficiency (SE). For example, all-ETDM based transmission at high baud rates in general does not allow sophisticated pulse shaping to obtain low roll-off Nyquist modulated spectra, limiting SE.

Transmission at high symbol rates can also be obtained using well known optical time division multiplexing (OTDM) techniques [2]. Recent works using orthogonal time division multiplexing of optical Nyquist pulses (Nyquist-OTDM) have demonstrated the possibility to obtain single carrier systems achieving both high symbol rate and Nyquist modulated spectra [3]. However, as conventional OTDM systems, such approaches generally require complicated synchronization and demultiplexing schemes employing optical phase-locked loop and nonlinear optical signal processing, respectively. For those reasons, its application has traditionally been limited to dispersion compensated links. Additionally, after data modulation, Nyquist-OTDM suffers from limited suppression ratio of the spectrum sidebands, since the overall resulting roll-off of the modulated spectrum depends on the number of TDM stages employed [4]. Spectra with sharp roll-offs after modulation are approximated by increasing the number of TDM tributaries. The complexity to build an OTDM system with large number of tributaries is not realistic, in general, for a network transceiver. However, for a reduced number of TDM stages, such technique may require guard bands between independent WDM channels [5]. Therefore, the SE will be reduced.

To avoid the mentioned limitations of pure ETDM and OTDM approaches, hybrid signal generation techniques have been proposed and experimentally demonstrated. In [7], a single channel, single polarization 125 GBd QPSK Nyquist-OTDM experiment employing full band signal coherent detection has been presented. Full field detection enables the receiver to demodulate the OTDM data with no additional requirement on the synchronization between transmitter and receiver. In [11] and [12], sub-band synthesis is employed to generate single carrier 124 GBd DP-32QAM and 128 GBd DP-16QAM, respectively, with low roll-off Nyquist spectral shaping. Hybrid techniques have a potential to overcome the bottlenecks of each individual approach, splitting the overall signal generation complexity between electrical and optical domains.

In this paper, we propose and experimentally demonstrate a hybrid approach allying optical generation of periodic sinc pulses and electrical pulse shaping to obtain Nyquist modulated spectra at symbol rates > 100 GBd without the use of extra optical filtering. To investigate the benefits of the proposed approach, we demonstrate the first WDM Nyquist-OTDM signal generation based on periodic train of sinc pulses and electrical spectrum shaping. Straight line transmission of five 112.5 Gbd Nyquist-OTDM DP-QPSK channels is demonstrated, up to 640 km dispersion uncompensated links, with full-field coherent detection at the receiver. It is shown that such design strategy effectively improves the roll-off of the modulated OTDM signal, reducing the crosstalk penalty in baud-rate-spaced Nyquist-WDM systems.

2. Spectrum Shape of Nyquist-OTDM Signals

The Nyquist-OTDM techniques considered in this work are the ones based on the optical generation of periodic sinc pulses [4]. Such pulse trains can be orthogonally multiplexed in time, since they comply with the Nyquist criteria for zero intersymbol interference (ISI) [13]. Analytic derivations supporting the discussion presented in this section are shown in the Appendix.

2.1. Design Trade-Offs of Optical Pulse Shaping

A periodic train of sinc pulses in time domain corresponds to a set of equidistant discrete tones, all with the same amplitude and with linear phase relationship, in the frequency domain mapped by the Fourier transform, as illustrated in Fig. 1.

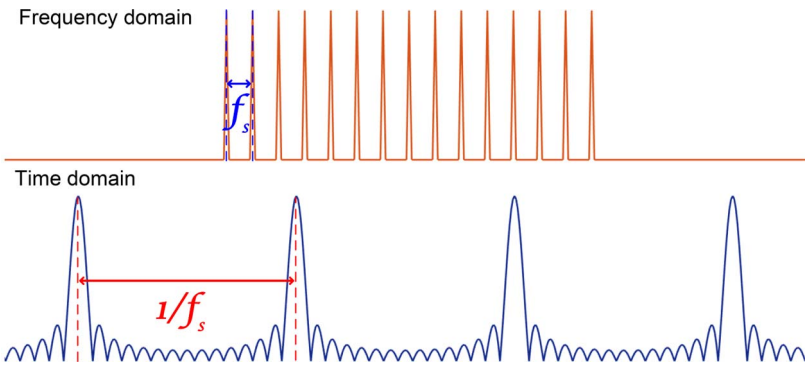

Fig. 1. Duality between flat comb in frequency and periodic sinc pulse train in time.

This property allows one to obtain a periodic train of sinc pulses by designing the correspondent frequency comb. The frequency comb can be essentially seen as the sampled version of a rectangular spectrum. As the frequency sampling resolution improves, i.e., the number of frequency tones within the rectangle bandwidth increases, the repetition rate of sinc pulses reduces and each individual pulse resembles better an ideal isolated sinc. The rectangle width defines the maximum serial baud rate that can be obtained after TDM.

A train of sinc pulses can be modulated at a symbol rate equal to the pulse repetition rate, which becomes also the base rate for TDM. In phase and quadrature (I/Q) linear modulation driven by standard square non return-to-zero (NRZ) electrical pulse shape does not affect the orthogonality between optical pulses in consecutive TDM slots. However, modulated trains of sinc pulses are no longer deterministic, but cyclostationary random processes [13]. Such modulation will result in an overall power spectral density (PSD) larger than the original sampled rectangular spectrum. This happens because the PSD of the process is dependent on the shape of the truncated sinc pulse modulated at each symbol period. Hence, the roll-off factor of the modulated spectra will actually depend on how good is the approximation of an infinite sinc obtained with the truncated pulse within each TDM slot. In other words, the sampling resolution of the rectangular spectrum approximated by the frequency comb defines the fidelity of an isolated sinc pulse in time, which determines the final roll-off of the modulated spectrum. Therefore, to obtain sharp roll-offs after modulation with such pulse generation technique, it is necessary to use frequency combs with large number of tones. As stated in [4], theoretically, such spectral broadening does not prevent WDM channels to be baud-rate-spaced without introducing crosstalk penalties. However, as a necessary condition to build such system, all WDM channels must be locked in frequency and phase, which is difficult to accomplish in practical WDM architectures. It should also be pointed that, in a real optical comb design, perfect suppression of side band harmonics usually cannot be achieved. Hence, such harmonics will also contribute to the spectral broadening after modulation.

Therefore, the modulation effect establishes a trade-off between SE and system complexity. To maximize SE, a low repetition rate is required for the sinc pulse train in order to minimize the roll-off factor of the final modulated spectrum. This implies in a large number of TDM stages, which increases the complexity of the transmitter. Additionally, increasing the number of comb tones will quickly raise the peak power values of the sinc pulses, which may bring further practical problems. On the other hand, increasing the repetition rate of the pulses to use a reduced number of TDM stages will result in a poor spectrum roll-off after modulation. Therefore, it would be beneficial to find a strategy where low roll-off factor Nyquist-OTDM modulated spectra can be generated using a reduced number of TDM stages, employing combs with few frequency tones.

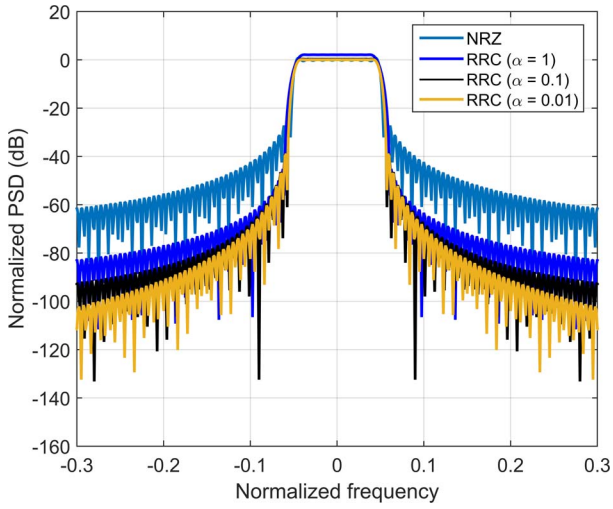

Fig. 2. Numerical comparison of Nyquist-OTDM spectra obtained with an ideal optical comb source with nine frequency tones, modulated with different electrical pulse shaping. The advantage of RRC over NRZ is clear in terms of sidelobe suppression.

2.2. Combined Optical and Electrical Spectrum Shaping

To overcome the complexity versus spectral confinement trade-off explained in the previous subsection, we propose a hybrid approach based on the combined effect of optical and electrical spectrum shaping. As detailed in Appendix, the electrical pulse shape $g(t)$ can be selected from a family of Nyquist pulses, like raised cosine (RC) or root raised cosine (RRC) pulses. Here, we have chosen to use RRC pulse shapes, due to its common use in communications. The replacement of the electrical square NRZ pulse shape, which is used to modulate the optical train of pulses by a RRC shape allows one to control the roll-off factor of the resultant modulated spectrum, independently of how many TDM stages are used to obtain the OTDM signal. RRC pulse shape is obtained with the use of finite impulse response (FIR) filters in the digital domain, and digital-to-analog converters (DACs). The effect of this change on the OTDM modulated spectrum is shown in Fig. 2. Since the pulse shaping done in the digital domain can be performed with a window of several symbol periods, the roll-off sharpness will not be limited by the shape of the optical truncated sinc pulse. Therefore, performing previous spectrum shaping on the electrical modulating signals should improve the spectral confinement of the final Nyquist-OTDM signals.

In order to experimentally verify the benefits of this approach, we built the setup described in Section 3.

3. Experimental Setup

The experimental setup is shown in Fig. 3. We should point first that, due to experimental convenience to generate a WDM system, the sinc pulse generator was positioned after the data modulation. In this case, the periodic sinc generation acts as pulse carver. However, one can show that the relevant mathematical operations describing pulse carving and modulation commute, so the order in which the two are carried out has no impact on the final result [see (12) and (13) in the Appendix].

At the transmitter side, an arbitrary waveform generator (AWG) with 64 GSa/s and 20 GHz bandwidth was used to generate either 7 or 12.5 GBd QPSK modulated signals, in order to obtain the symbol rates of 63 and 112.5 GBd, respectively, after OTDM. In order to perform pulse shaping on the baseband signal generated by the AWG, a RRC digital filter was used. The filter was configured in order to provide the roll-off values (α) of 0.01, 0.2, 0.5, or 1 for the baseband

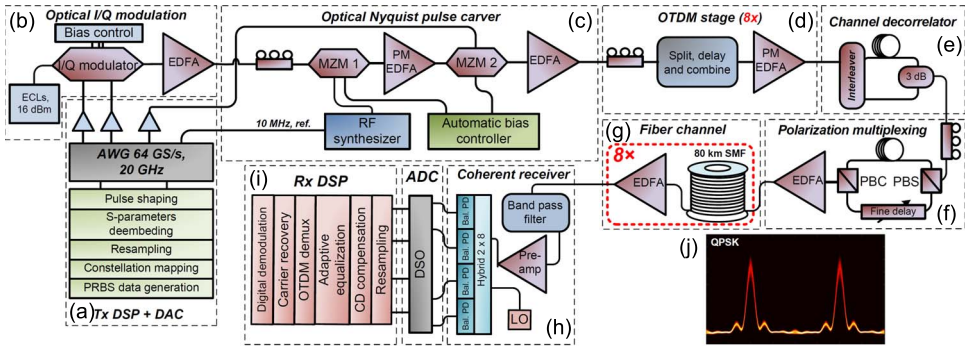

Fig. 3. Experimental setup used to generate five 112.5 GBd DP-QPSK Nyquist-OTDM channels. (a) Transmitter DSP, ADC conversion, and linear electrical amplification. (b) Optical I/Q modulation. (c) Periodic sinc pulse carving. (d) Delay and add OTDM emulation. (e) Decorrelation of WDM channels. (f) Polarization multiplexing emulation stage. (g) Straight line fiber channel with EDFA only amplification. (h) Coherent receiver frontend. (i) Receiver's offline DSP. (j) QPSK eye diagram of the signal before the OTDM stage.

spectrum. The electrical signal was then amplified to drive an optical I/Q modulator. The optical input to the modulator was provided by an array of free-running continuous wave (CW) external cavity lasers (ECLs) with 100 kHz linewidth. For the single channel characterization, one laser centered at 193.4 THz was used, while for the WDM case, five lasers centered at 192.625 THz, with spacing varied between 100 and 200 GHz in steps of 12.5 GHz, were used. The modulated signal was then sent to the Nyquist pulse carver (cf. eye diagram inset in Fig. 3). Both Mach-Zehnder modulators (MZMs) were driven by two RF sources synchronized with 10 MHz reference clock, with the second MZM driven by a sinusoidal clock generated by the AWG at a frequency equal to the base symbol rate i.e., 7 or 12.5 GHz, and the first MZM with this frequency tripled, i.e., 21 or 37.5 GHz. An automatic bias control for MZMs enabled stability and flatness of the frequency tones. Nine spectral lines composed the comb, resulting in a sinc pulse repetition after each nine consecutive zero crossings in time domain. Therefore, such configuration provided nine time multiplexing slots, allowing Nyquist-OTDM maximum aggregated serial rates of 63 and 112.5 GBd per channel. This signal was then fed to a three-stage OTDM multiplexer, where in each stage the signal was split, delayed and recombined. Since the multiplexer was only able to fill 8 TDM slots, one slot was left empty. Therefore, the effective transmission rates in Gb/s for the 63 GBd and 112.5 GBd test cases were 224 Gb/s and 400 Gb/s per channel, respectively. However, the spectral width of both modulated signals is not affected by the empty slot, hence corresponding to 63 GHz and 112.5 GHz in the Nyquist limit (see the Appendix). For the WDM transmission, the signal passed through a flex-grid interleaver, in order to decorrelate WDM channels after modulation with a single modulator. The OTDM signal was then passed to the polarization multiplexer, where it was combined with its delayed copy in the orthogonal polarization. For the experiment involving fiber transmission, the signal was sent to a fiber link composed of up to eight SSMF spans of 80 km each, with Erbium-doped fiber amplifiers (EDFAs) compensating losses after each span. The launch power was kept at 0 dBm per channel. After passing through the fiber link, the signal was pre-amplified, sent to a 0.9 nm optical bandpass filter and detected by a 40 GHz coherent receiver, using an ECL with 100 kHz linewidth as local oscillator. A real-time sampling oscilloscope with 33/63 GHz analog bandwidth per channel and sampling rate of 80/160 GSa/s was used to sample the 63/112.5 GBd signals. As only two 63 GHz inputs were available in the oscilloscope, only one polarization of the 112.5 GBd signal was digitized at the receiver and the incoming signal was appropriately aligned by a polarization controller. A set of coherent DSP algorithms [8], consisting of resampling, chromatic dispersion compensation, timing recovery, polarization demultiplexing and equalization, digital OTDM tributary demultiplexing, and carrier frequency, and phase recovery with an extended Kalman filter [9], was used to perform signal demodulation.

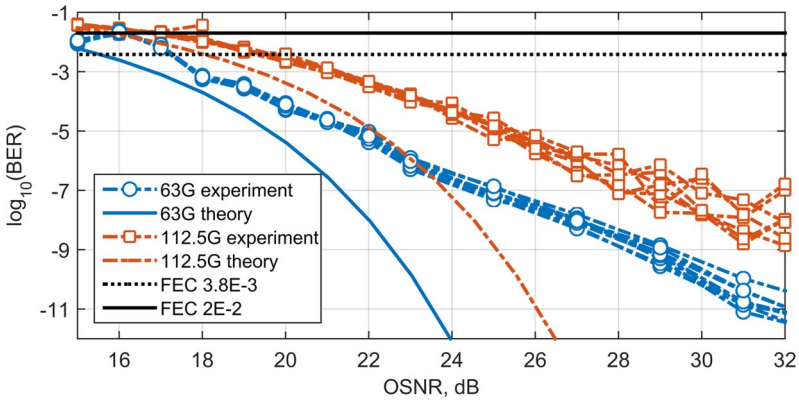

Fig. 4. Back-to-back performance curves for 63 GBd and 112.5 GBd DP-QPSK.

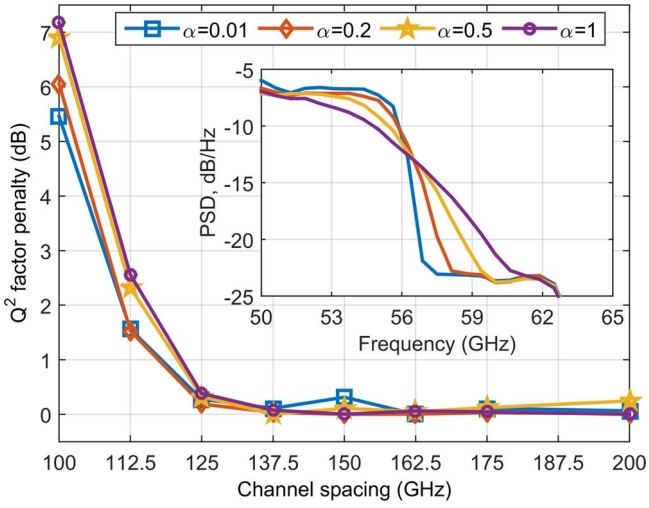

Fig. 5. Crosstalk penalty on the central channel performance as function of the carrier spacing for the back-to-back WDM configuration consisting of five 112.5 GBd DP-QPSK channels. The values for carrier spacing were chosen in agreement with the ITU flexigrid standard.

4. Results

Fig. 4 shows the single channel back-to-back performance for 63 and 112.5 GBd DP-QPSK, with implementation penalties of 2 dB for both cases, at the BER threshold of 3.8×10^{-3} for the 7% overhead hard FEC. The curves depicted represent a superposition of the average BER of each OTDM tributary. The bit error rate (BER) values below 10^{-5} were estimated from the error vector magnitude (EVM), calculated from the received constellation after carrier recovery.

The inset plot in Fig. 5 shows a magnified positive side of the single carrier baseband spectrum, around the symbol rate boundary (56.25 GHz), for all investigated values of α. This plot shows how the spectrum confinement is improved as α decreases. Lowering α largely suppresses spectral leakage from neighboring WDM channels and, thus, reduces inter-channel crosstalk for baud rate spacing [5]. The main plot in Fig. 5 shows the performance penalty due to crosstalk on the central channel for different values of α of the electrical RRC shaping for 112.5 GBd DP-QPSK. For each α chosen, the penalty is calculated with respect to the best Q^2-factor obtained when the carriers are enough spaced ($\geq$ 150 GHz) to safely disregard

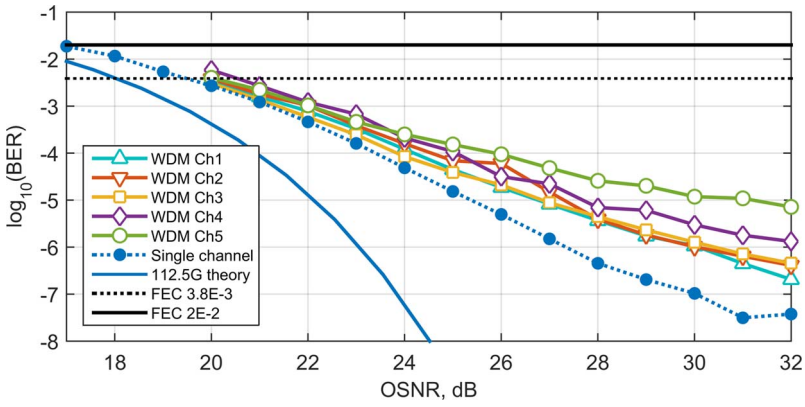

Fig. 6. Back-to-back performance of all five channels for the WDM 112.5 GBd DP-QPSK configuration.

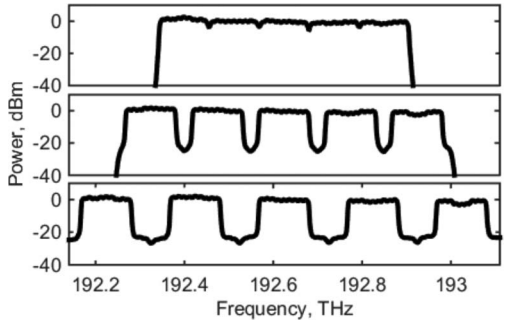

Fig. 7. Spectrum of the modulated optical carriers for three different channel spacings (a) 112.5 GHz (baud rate spacing). (b) 125 GHz. (c) 200 GHz.

crosstalk penalties. It is shown that, for baud rate channel spacing, lower values of α result in lower crosstalk penalty. The lowest penalty at baud rate spacing is 1.5 dB, which is close to the optimum values obtained for baud rate spaced Nyquist-WDM systems based on digital filtering only [14]. A drawback of this technique is the fact that, when α is reduced, there is an increase of the peak-to-average power ratio (PAPR) on the AWG outputs [6], which leads to increased implementation penalty. Therefore, further investigation is needed in order to quantify the trade-off between crosstalk suppression and PAPR penalty.

Fig. 6 shows the back-to-back BER performance for all WDM channels in comparison to the performance of a single channel. Each plotted value corresponds to average BER of all OTDM tributaries. A WDM implementation penalty of 2 dB for the best WDM channel is observed. Performance varies across different WDM channels due to non-flat noise floor at higher optical SNRs as well as slight dependence of the Nyquist carver modulators bias on the wavelength, leading to suboptimal Nyquist pulse generation for outer channels. This is also visible in Fig. 7, which depicts optical spectra for the WDM channel spacing of 112.5 GHz, 150 GHz, and 200 GHz. Particularly at a spacing of 200 GHz, this dependence can be easily observed in the uneven spectra of non-central WDM channels.

Fig. 8 shows five-channel WDM Nyquist-OTDM 112.5 GBd DP-QPSK back-to-back transmission performance, with $\alpha = 1$ and channel grid spacing of 125 GHz. The grid spacing was set to 125 GHz, instead of 112.5 GHz, due to the limitations of the WaveShaper used to emulate a WDM optical interleaver on the channel decorrelator (see Fig. 3). Since it was not possible to create an attenuation profile to demultiplex and decorrelate even and odd channels at

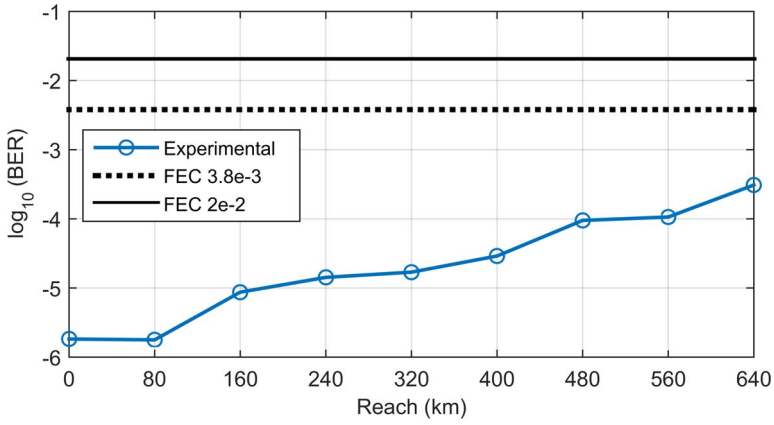

Fig. 8. Transmission performance over straight line SSMF spans for the central channel in the WDM configuration. The indicated BER is the average value of all OTDM tributaries.

112.5 GHz, the solution found was to increase the channel grid by 12.5 GHz, in order to keep the agreement with the ITU flexigrid standard [15]. The choice of α was made in order to minimize a possible impact of PAPR on the transmission results. The WDM transmission was successfully performed up to 640 km spans of straight line dispersion uncompensated fiber link. The launched power per channel was set to 0 dBm, in order to guarantee that the system would operate in the linear regime. The OSNR value of 23.2 dB per carrier was measured after 640 km of transmission. As the measured performance was the same obtained in back-to-back, for identical OSNR value, it indicates that the linear fiber impairments where completely compensated after DSP, adding no penalty to the system performance. Additional investigation is required to evaluate optimum launch power per channel, which was roughly estimated around 4 dBm on this experiment, and the maximum transmission reach, which clearly was limited by the amount of fiber available in straight line setup. One should point out that the performance results presented in Fig. 8 may be *underestimated*, since only one polarization of the signal is being acquired and processed at the time. Better performances should be expected with the use of a complete dual polarization coherent receiver for the 112.5 Gbd setup, which would allow optimal equalization of the polarization mixing effects. Additionally, the BER values obtained in a sub-optimal scenario are low enough to guarantee that the results can be reproduced with the complete dual polarization receiver.

5. Conclusion

We have shown that, by allying optical generation of periodic sinc pulses and electrical pulse shaping, the roll-off factor of the OTDM modulated spectrum can be reduced, independently of the number of optical comb lines used to generate the periodic train of sinc pulses. The proposed approach can balance the complexity of the transmitter between optical and electrical domains, enabling the generation of Nyquist modulated channels at symbol rates > 100 GBd, without the use of any bandpass optical filter for sidelobe suppression. The benefits of this approach are experimentally quantified, showing that inter-channel crosstalk penalty can be reduced up to 1.5 dB at baud rate spacing of 112.5 Gbd DP-QPSK channels. Additionally, based on this technique, we successfully demonstrated the first WDM generation and straight line dispersion uncompensated transmission of five 112.5 Gbd DP-QPSK Nyquist-OTDM carriers over 640 km with full-field coherent detection at the receiver. Results show that this approach can be suitable to design low roll-off, high baud rate Nyquist transceivers. Further investigation is needed to quantify the impact of PAPR induced by the electrical pulse shaping and the performance for higher order modulation formats.

Appendix
Analytic Derivation of the Spectrum Shaping Relations Between Optical and Electrical Domains

Equation (1) is a known result from the Fourier analysis of periodic functions. The inverse Fourier transform of an infinite periodic sequence of impulses in the frequency domain $P(f)$ with period f_s corresponds to an infinite periodic sequence of impulses in time domain $p(t)$ with period $T_s = 1/f_s$

$$P(f) = \frac{1}{T_s}\sum_{n=-\infty}^{\infty}\delta(f - nf_s) \Longleftrightarrow p(t) = \sum_{n=-\infty}^{\infty}\delta(t - nT_s) \tag{1}$$

where n is an integer number. In order to select an odd number of N frequency tones centered around 0 frequency $P_N(f)$ from the infinite sequence $P(f)$, we define a rectangular window $R(f)$ in frequency domain and its correspondent inverse Fourier function in time

$$R(f) = \begin{cases} 1, & |f| \le \frac{Nf_s}{2} \\ 0, & |f| \ge \frac{Nf_s}{2} \end{cases} \Longleftrightarrow r(t) = N\ \text{sinc}\ (Nf_s t) \tag{2}$$

where $\text{sinc}(x) = \sin(\pi x)/\pi x$.

Therefore, using the equivalence between convolution in the time domain and multiplication in the frequency domain, we can write

$$P_N(f) = R(f)P(f) \Longleftrightarrow p_N(t) = r(t) * p(t) \tag{3}$$

$$p_N(t) = N\ \text{sinc}\ (Nf_s t) * \sum_{n=-\infty}^{\infty}\delta(t - nT_s) \tag{4}$$

$$p_N(t) = \sum_{n=-\infty}^{\infty} N\ \text{sinc}[Nf_s(t - nT_s)]. \tag{5}$$

If the bandwidth of the rectangular window is fixed in $B = Nf_s$, we have $N = B/f_s$. Replacing it in (5), we have

$$p_N(t) = \sum_{n=-\infty}^{\infty}\frac{B}{f_s}\text{sinc}\left[\frac{B}{f_s}\left(\frac{t}{T_s} - n\right)\right]. \tag{6}$$

Equation (6) represents a periodic train of sinc pulses in the time domain, generated by a comb with $N = B/f_s$ frequency components. The repetition rate of consecutive sinc pulses is equal to f_s, and the number of zero crossings between two consecutive pulse peaks is given by N. In order to obtain the equivalent expression considering an even number of comb lines, the same steps can be used. To simplify the calculations using properties of the Fourier transform, $P(f)$ should be shifted by $f_s/2$ in order to have both impulse train and rectangular window symmetric with respect to $f = 0$. This operation does not affect the generality of the result. We then have

$$P_N(f) = R(f)P(f - f_s/2) \Longleftrightarrow p_N(t) = r(t) * p(t)e^{j\pi f_s t} \tag{7}$$

$$p_N(t) = N\ \text{sinc}\ (Nf_s t) * \sum_{n=-\infty}^{\infty} e^{j\pi f_s t}\delta(t - nT_s) \tag{8}$$

$$p_N(t) = \sum_{n=-\infty}^{\infty} e^{j\pi n} N\ \text{sinc}\ [Nf_s(t - nT_s)] \tag{9}$$

$$p_N(t) = \sum_{n=-\infty}^{\infty}(-1)^n\frac{B}{f_s}\text{sinc}\left[\frac{B}{f_s}\left(\frac{t}{T_s} - n\right)\right]. \tag{10}$$

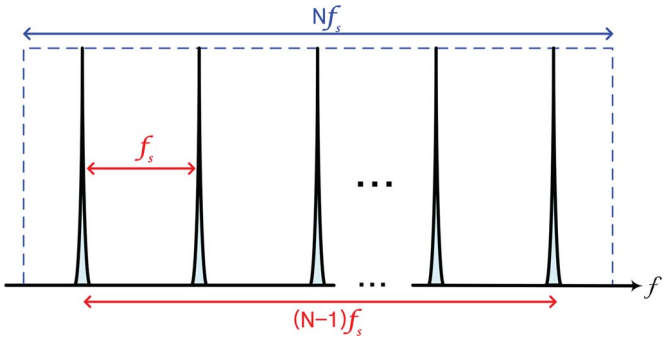

Fig. 9. Ideal frequency comb with N tones spaced by f_s Hz, resembling a sampled rectangular spectrum with bandwidth Nf_s Hz.

A general formula for both cases is summarized as follows:

$$p_N(t) = \sum_{n=-\infty}^{\infty} (-1)^{(B/f_s-1)n} \frac{B}{f_s} \text{sinc}\left[\frac{B}{f_s}\left(\frac{t}{T_s} - n\right)\right]. \tag{11}$$

Consider the case where the optical pulse train is modulated by applying a linear memoryless M-ary modulation format with unitary average symbol energy. Assuming an electrical pulse shape $g(t)$, with Fourier transform $G(f)$, the equivalent low-pass complex modulated signal $s(t)$ and its corresponding power spectral density $\Phi_s(f)$ will be given, respectively, by

$$s(t) = \sum_{k=-\infty}^{\infty} A_k e^{j\phi_k} g(t - kT_s) p_N(t - kT_s) \tag{12}$$

$$\Phi_s(f) = \frac{1}{T_s} |G(f) * P_N(f)|^2 \tag{13}$$

where $A_k e^{j\phi_k}$ represent the symbol transmitted at the $t = kT_s$ instant. From (13), we can easily see that the final bandwidth of the modulated signal (B_S) will be given by the sum of bandwidth of the optical comb (B_{P_N}) with the bandwidth of the electrical pulse (B_G). As depicted in Fig. 9, we have $B_{P_N} = (N-1)f_s$. It follows that

$$B_S = (N-1)f_s + B_G \geq B = Nf_s \tag{14}$$

where the equality holds at the Nyquist limit. Therefore, in the Nyquist limit, $B_G = f_s$. Since $G(f)$ is independent of N, so is the final roll-off of the modulated spectrum. Additionally, it is shown that is possible to obtain low roll-offs for Nyquist-OTDM signals, even when N is a small number.

References

[1] G. Raybon, S. Randel, A. Adamiecki, and P. J. Winzer, "High symbol rate transmission systems for data rates above 400 Gb/s using ETDM transmitters and receivers," in *Proc. IEEE ECOC*, 2014, pp. 1–3.
[2] T. Richter, M. Nolle, F. Frey, and C. Schubert, "Generation and coherent reception of 107-GBd optical Nyquist BPSK, QPSK, and 16QAM," *IEEE Photon. Technol. Lett.*, vol. 26, no. 9, pp. 877–880, May 2014.
[3] D. O. Otuya, K. Kasai, M. Yoshida, T. Hirooka, and M. Nakazawa, "Single-channel 1.92 Tbit/s, Pol-Mux-64 QAM coherent Nyquist pulse transmission over 150 km with a spectral efficiency of 7.5 bit/s/Hz," *Opt. Exp.*, vol. 22, no. 20, pp. 23 776–23 785, Oct. 2014.
[4] M. A. Soto *et al.*, "Optical sinc-shaped Nyquist pulses of exceptional quality," *Nat. Commun.*, vol. 4, pp. 1–13, 2013.
[5] A. J. Lowery, C. Zhu, E. Viterbo, and B. Corcoran, "All-optical generation of DFT-S-OFDM superchannels using periodic sinc pulses," *Opt. Exp.*, vol. 22, no. 22, pp. 27 026–27 041, Nov. 2014.
[6] R. Schmogrow *et al.*, "Real-time Nyquist pulse generation beyond 100 Gbit/s and its relation to OFDM," *Opt. Exp.*, vol. 20, no. 1, pp. 317–337, 2012.
[7] J. Zhang, J. Yu, Y. Fang, and N. Chi, "High speed all optical Nyquist signal generation and full-band coherent detection," *Sci. Rep.*, vol. 4, 2014, Art. ID 6156.

[8] R. Borkowski, D. Zibar, and I. T. Monroy, "Anatomy of a digital coherent receiver," *IEICE Trans. Commun.*, vol. E97-B, no. 8, pp. 1528–1536, 2014.
[9] D. Zibar *et al.*, "Application of machine learning techniques for amplitude and phase noise characterization," *J. Lightw. Technol.*, vol. 33, no. 7, pp. 1333–1343, Apr. 2015.
[10] G. Bosco *et al.*, "Investigation on the robustness of a Nyquist-WDM terabit superchannel to transmitter and receiver non-idealities," in *Proc. IEEE ECOC*, 2010, pp. 1–3.
[11] R. Rios-Müller *et al.*, "1-Terabit/s net data-rate transceiver based on single-carrier Nyquist-shaped 124 Gbaud PDM-32QAM," in *Proc. IEEE OFC*, 2015, pp. 1–3.
[12] H. Mardoyan *et al.*, "Transmission of single-carrier Nyquist-shaped 1-Tb/s line-rate signal over 3,000 km," in *Proc. IEEE OFC*, 2015, pp. 1–3.
[13] J. Proakis, *Digital Communications*, 4th ed. New York, NY, USA: McGraw-Hill, Aug. 2000.
[14] R. Maher *et al.*, "Digital pulse shaping to mitigate linear crosstalk in Nyquist-spaced 16QAM WDM transmission systems," in *Proc. OptoElectron. Commun. Conf. Australian Conf.*, 2014, pp. 76–78.
[15] "Spectral grids for WDM applications: DWDM frequency grid," Int. Telecommun. Union (ITU), Geneva, Switzerland, Recommendation ITU-T G.694.1, Feb. 2012.